Journal of Applied Fluid Mechanics, Vol. 10, No. 1, pp. 413-420, 2017.
Available online at www.jafmonline.net, ISSN 1735-3572, EISSN 1735-3645.
DOI: 10.18869/acadpub.jafm.73.238.26142

Three-Dimensional Axisymmetric Solidification of a Viscous Incompressible Flow in the Stagnation Point Region

A. Shokrgozar Abbasi

Department of Mechanical Engineering, Payame Noor University, Iran

Email: shokrgozar.ali@gmail.com

(Received January 23, 2016; accepted May 25, 2016)

ABSTRACT

The history of the study of fluid solidification in stagnation flow is very limited. Among these studies, only one two-dimensional Cartesian coordinate case has considered fluid viscosity and pressure variation along the boundary layer. In the present paper, the solidification process of an incompressible viscous fluid in a three-dimensional axisymmetric coordinate system is considered. The solidification is modeled by solving the momentum equations governing a problem in which a plate is moving toward an impinging fluid with a variable velocity and acceleration. The unsteady momentum equations are transformed to ordinary differential equations by using properly introduced similarity variable. Furthermore, pressure variations along the boundary layer thickness are taken into account. The energy equation is solved by numerical method as well as similarity solution. Interestingly, similarity solution of the energy equation is used for validation of the numerical solution. In this research, distributions of the fluid temperature, transient distributions of the velocity components and, most importantly, the solidification rate are presented for different values of non-dimensional governing parameters including Prandtl number and Stefan number. A comparison is made between the solidification processes of axisymmetric three-dimensional and two-dimensional cases to justify the achieved results in a better way. The obtained results reveal that there is a difference between the final solid thickness, when the process has reached to its steady condition, of three-dimensional axisymmetric and two-dimensional cases. Also the results show that increase the Prandtl number up to 10 times or increase the heat diffusivity ratio up to 2 times lead to decrease the ultimate frozen thickness almost by half. While, the Stefan number has no effect on the value of thickness and its effect is captured only on the freezing time. Prediction the ultimate thickness of solid before obtaining solution and introducing a new method for validation of numerical results are achievements in this research.

Keywords: Axisymmetric solidification; Viscous flow; Exact solution; Stagnation point; Unsteady flow.

NOMENCLATURE

$a(t)$	time-dependent potential flow strain rate
$a_\circ$	potential flow Strain rate at time
f	similarity function
h_{ls}	solidification latent heat
k_r	ratio of K
Pe	Pecklet number
Pr	Prandtl number
$S(t)$	solid phase thickness
$\widetilde{S}$	non-dimensional solid thickness
St	Staefan number
T	Temperature
t	Time
α_r	ratio of α
η	similarity variable, non-dimensional Z axis
μ	Viscosity
θ	non-dimensional temperature,
τ	non-dimensional time
ξ	non-dimensional r axis
ζ	variable
ρ	Density
ν	kinetic viscosity

Subscripts

I,i	initial temperature of fluid at potential flow
J	Liquid

1. INTRODUCTION

Solidification is a two-phase phenomenon that is used in different natural processes and industrial applications. Glass, metal, plastic and oil industries, providing food and other corresponding industries needs a good insight of solidification behavior as the nature of solid growth.

Studies of phase change in stagnant media for better understanding of convection effect upon the interface behavior and solidification properties are needed by industrial demand such as the desire for more homogenous semi-conductor crystals, in nuclear industry, as well as the better understanding of natural ice formation.

The classic problem stagnant fluid solidifying on the cold plate is solved (Stefan 1951). One dimensional heat fluxes method for phase change problem is presented (Goodrich 1978). These methods are accompanied simplified assumptions such as one dimensionality solid-liquid interface. An experimental study for natural convection in interface within heat flux controlling due to solidification is provided (Sparrow and Ramsey and Harris 1983). Also a numerical method for solidifying in natural convection is used (Lacroix 1989) and three dimensional problems for natural convection accompaniment phase change in rectangular channel is solved (Hadji and Schell 1990) in fluid variable properties state with temperature. Solidification of a fluid layer confined between two isolated plates is investigated (Hanumanth 1990). Another way for calculating of heat flux depended to on time in natural convection is presented (Curtic and Oldenburg and Frank 1992). A combined model for phase change upon various states of pure substances, melting fluid problem due to spreading and solidifying on the flat plate and numerical modeling of forming and solidifying of a droplet on a cold plate is investigated (Trapaga *et al.*. 1992; Watanabe *et al.*. 1992; Marchi *et al.*. 1993). Evolution due to impact on substrate plate and solidifying of a droplet (Brattkus and Davis 1988) is presented. But in concentrating upon stagnation flow, solidification of an inviscid fluid at interface and effect of its phenomena on morphological instability is investigated (Rangel and Bian 1994). Stefan problem for inviscid stagnation flow by two methods and solidifying of super-cooled liquid stagnation inviscid flow is considered (Lambert and Rangel 2003; Yoo 2000), respectively. Recently, the two-dimensional solidification of a viscous stagnation flow has considered (Shokrgozar and Rahimi 2013). In this article, the exact solution of the momentum equations (Shokrgozar and Rahimi 2012) is used for numerical solution of the energy equation. Imagine the fluid from far field moves perpendicularly approaches to a cold plate and after impinging on the plate the solid phase will formed on it gradually (Figure 1).

In this study, the solidification process of a viscous stagnation flow is investigated in a three-dimensional axisymmetric coordinate where a new method is implemented for validation of the numerical results. In this method, the exact solution of a heat profile is used as a quasi-steady solution for the problem. A parametric study is performed to examine influences of governing dimensionless parameters on the results as well. An exact solution is performed for solving momentum equations (Shokrgozar and Rahimi and Mozayyeni 2016) while the energy equation in liquid phase, solid-liquid interface and solid phase is solved by using finite difference method. The exact solution of the energy equation is used for validation of the numerical solution of energy equation, too. Forth order Runge-Kutta algorithm is used for solving momentum and energy equations. In addition, Numerical solution is needed to finding unsteady temperature profiles at each time step.

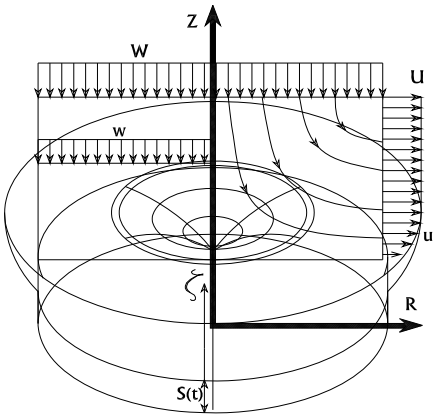

Fig. 1. Axisymmetric stagnation flow (coordinate system).

2. PROBLEM FORMULATION

Figure 1 represents three-dimensional axisymmetric coordinates with corresponding (u,w) velocities related to (r,z). A viscous laminar unsteady incompressible stagnation flow with strain $a(t)$ perpendicularly approaches to a plate, along z-direction, initially positioned at $z=0$ when $t=0$. For all times of consideration, the fluid is solidified with variable solidification velocity and acceleration, $\dot{S}(t)$ and $\ddot{S}(t)$, respectively, that of an imaginary plate at solid-liquid interface is moved towards fluid where $S(t)$ is the plate distance, at time t, from the plate origin at $z=0$. In later section, we will see why the imaginary plate is considered as a flat one because the only mechanism of heat transfer in the interface is conduction with the same temperature difference so the substrate remains flat. Notice that the inviscid flow can be assumed as potential flow within displacement thickness in boundary layer region. In reference (Shokrgozar *et al.*, 2013), more explanations were given regarding the strain variations. Note a_0 is the strain rate at far field.

For a Newtonian fluid with constant density and viscosity, unsteady three-dimensional axisymmetric

Navier-Stokes equations governing the flow and heat transfer are given as:

Mass:

$$\frac{1}{r}\frac{\partial}{\partial r}(r u)+\frac{\partial w}{\partial z}=\circ \tag{1}$$

Momentum:

$$\frac{\partial u}{\partial t}+u\frac{\partial u}{\partial r}+w\frac{\partial u}{\partial z}= =-\frac{1}{\rho}\frac{\partial p}{\partial r}+\upsilon\left(\frac{\partial^2 u}{\partial r^2}+\frac{1}{r}\frac{\partial u}{\partial r}-\frac{u}{r^2}+\frac{\partial^2 u}{\partial z^2}\right) \tag{2}$$

$$\frac{\partial w}{\partial t}+u\frac{\partial w}{\partial r}+w\frac{\partial w}{\partial z} =-\frac{1}{\rho}\frac{\partial p}{\partial z}+\upsilon\left(\frac{\partial^2 w}{\partial r^2}+\frac{1}{r}\frac{\partial w}{\partial r}+\frac{\partial^2 w}{\partial z^2}\right) \tag{3}$$

In liquid phase:

Energy (dissipation and radiation heat transfer are neglected without internal source):

$$\frac{\partial T}{\partial t}+u\frac{\partial T}{\partial r}+w\frac{\partial T}{\partial z}=\alpha\left[\frac{\partial^2 T}{\partial r^2}+\frac{1}{r}\frac{\partial T}{\partial r}+\frac{\partial^2 T}{\partial z^2}\right] \tag{4}$$

In solid phase:

$$\frac{\partial T}{\partial t}=\alpha\left[\frac{\partial^2 T}{\partial r^2}+\frac{1}{r}\frac{\partial T}{\partial r}+\frac{\partial^2 T}{\partial z^2}\right] \tag{5}$$

At interface:

$$\rho h_{ls}\frac{d S(t)}{d t}=k_s\frac{\partial T_s}{\partial z}-k_l\frac{\partial T_l}{\partial z} \tag{6}$$

Notice, conductivity and heat capacity coefficients are constant (*k* and *c* respectively) also $du \approx c\,dT$ is assumed where p, ρ, υ, and α are the fluid pressure, density, kinematic viscosity, and thermal diffusivity, respectively. The dissipation terms are neglected in the energy equation because of the flow velocities being too small. Also, subscripts s and l denote solid and liquid, respectively.

3. SOLUTION

3.1. Fluid Flow Similarity Solution

According to (Shokrgozar Abbasi 2016), viscous parts of the velocity components are as:

$$u=a(t)\,r\,f'(\eta) \tag{7}$$

$$w=-2\sqrt{\upsilon/a_\circ}\;a(t)\,f(\eta) \tag{8}$$

$$\eta=\sqrt{\upsilon/a_\circ}\,\zeta \quad ,and \quad \zeta=z-S(t) \tag{9}$$

In which the terms involving $f(\eta)$ in (7), (8) comprise the axisymmetric similarity form for unsteady stagnation flow, and prime denotes differentiation with respect to η. Transformations (7)-(9) satisfy (1) automatically and their insertion into (2)-(3) yields an ordinary differential equation in terms of $f(\eta)$ along with an expression for the pressure, as follow:

$$f'''+f''\left(\tilde{\dot{S}}+2\tilde{a}\,f\right)+\left(-\tilde{a}\;f'-\frac{1}{\tilde{a}}\frac{d\tilde{a}}{d\tau}\right)f' -\frac{1}{\tilde{a}}\frac{1}{\xi}\frac{\partial\tilde{P}}{\partial\xi}=0 \tag{10}$$

$$\tilde{p}-\tilde{p}_\circ=-2\tilde{a}\left(\tilde{a}f^2+f'+\tilde{\dot{S}}f\right) -\frac{\xi^2}{2}\left(\frac{\partial\tilde{a}}{\partial\tau}+\tilde{a}^2\right)+\int_0^\eta 2\frac{\partial\tilde{a}}{\partial\tau}\,f\,d\eta \tag{11}$$

In which:

$$-\frac{1}{\tilde{a}}\frac{1}{\xi}\frac{\partial\tilde{P}}{\partial\xi}=\frac{1}{\tilde{a}}\frac{\partial\tilde{a}}{\partial\tau}+\tilde{a} \tag{12}$$

$$\frac{\partial\tilde{a}}{\partial\tau}=\frac{\tilde{\dot{S}}}{\eta_\circ}+\frac{\tilde{\dot{S}}^2}{\eta_\circ^2}+\frac{\tilde{W}_\circ\tilde{\dot{S}}}{\eta_\circ^2} \tag{13}$$

$$\tilde{P}(r,z,t)=\frac{p(r,z,t)}{\rho a_\circ\upsilon}\;,\quad \tilde{S}(t)=\sqrt{a_\circ/\upsilon}\,S(t)$$
$$\tilde{a}(t)=\frac{a(t)}{a_\circ}\;,\quad \tilde{\dot{S}}(t)=\dot{S}(t)/\sqrt{a_\circ\,\upsilon}\;,\quad \xi=\sqrt{a_\circ/\upsilon}\;r \tag{14}$$

Where dot denotes differentiation with respect to t, Also, $\tilde{P},\tilde{S},\tilde{\dot{S}}$ and $\tilde{r}$ are dimensionless forms of $P,S,\dot{S}$ and r, respectively.

The boundary conditions for the differential equation (10) are:

$$\eta=\circ:\quad f=0,\quad f'=0 \tag{15}$$

$$\eta\to\infty:\quad f'=1 \tag{16}$$

It is worth mentioning that relation (11) which represents pressure is obtained by integrating Equation (3) in z-direction and by use of the potential flow solution as boundary conditions.

3.2.1 Exact Solution of Heat Transfer

To transform the energy equation into a non-dimensional form for the case of defined wall temperature, we introduce:

$$\theta=\frac{T(\eta)-T_\infty}{T_w-T_\infty} \tag{17}$$

Making use of transformations (7) - (9), this equation may be written as:

$$\theta''+\left(\tilde{\dot{S}}(\tau)+2\;f\right)Pr.\theta'=0 \tag{18}$$

With boundary conditions as:

$$\eta=0:\qquad \theta=1 \tag{19}$$

$$\eta\to\infty:\qquad \theta=0 \tag{20}$$

Where θ is dimensionless temperature, the subscript w and ∞ refer to the conditions at the wall and in the free stream, respectively, and prime indicates differentiation with respect to η.

3.2.2 Numerical Heat Transfer Solution

Using the non-dimensional quantities for temperature as θ, time as τ, distance from r axis as $\tilde{r}$, and distance from z axis as $\tilde{z}$, equations (4)-(6) become:

For liquid phase:

$$\frac{\partial \theta_l}{\partial \tau}+\tilde{u}\frac{\partial \theta_l}{\partial \tilde{r}}+\tilde{w}\frac{\partial \theta_l}{\partial \tilde{z}}=\alpha_l\left(\frac{\partial^2 \theta_l}{\partial \tilde{r}^2}+\frac{1}{\tilde{r}}\frac{\partial \theta_l}{\partial \tilde{r}}+\frac{\partial^2 \theta_l}{\partial \tilde{z}^2}\right) \quad (21)$$

For solid phase:

$$\frac{\partial \theta_s}{\partial \tau}=\alpha_s\left(\frac{\partial^2 \theta_s}{\partial \tilde{r}^2}+\frac{1}{\tilde{r}}\frac{\partial \theta_s}{\partial \tilde{r}}+\frac{\partial^2 \theta_s}{\partial \tilde{z}^2}\right) \quad (22)$$

And for their intersection:

$$\frac{Pr}{St}\frac{d\tilde{S}}{d\tau}=\frac{1}{k_r}\frac{\partial \theta_s}{\partial \tilde{z}}-\frac{\partial \theta_l}{\partial \tilde{z}} \quad (23)$$

4. SOLUTION METHOD

At first, the momentum equation of liquid (10) is solved numerically using a shooting method based on Runge-Kutta algorithm. Resulted velocities are used in energy equation (21) in liquid region in order to convert this nonlinear equation to a linear one. Then this linear equation is dischretized by using Power Law scheme so for small $Pe(Pe<1)$ and Large $Pe(Pe>10)$, scheme is central and upwind, respectively. For $1<Pe<10$, scheme is composite of these two. For solving the algebraic system of equations, TDMA (Three Diagonal Matrix Algorithm) within ADI (Alternating Direction Implicit) method is used. In addition, the resulted velocities of momentum solution are used to obtain the exact solution of energy equation (Shokrgozar *et al.*, 2016). However, this exact solution is not used to capture the fluid temperature in the computational domain at each time step. In the next sections, the reason of this phenomenon will be discussed.

5. VALIDATION AND PRESENTATION OF RESULTS

In this section, in order to validate the energy equation numerical results of our study, the obtained results are compared with exact solution and previous studies. Comparison of results between this study and exact solution is new and creative method. For comparisons, (Shokrgozar *et al.*, 2013) study results are the most complete study and best selection. This reference was selected to validate the achieved results. For simplification and more excellent comparisons, parameter introducing in this study is the same as (Shokrgozar *et al.*, 2013) study. The results of these two studies are presented together in figure 3 for $(Pr=1,\ St=1,\ \theta_i=1,\ \alpha_r=1,\ k_r=1)$.

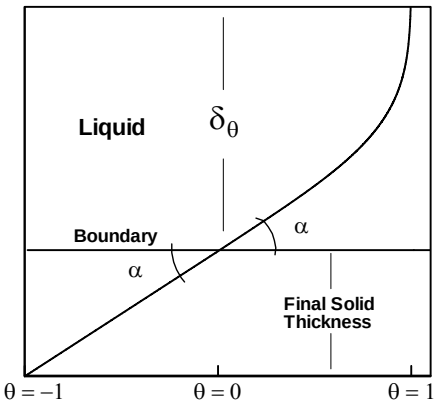

Fig. 2. a Final solid thickness, Low *Pr* number.

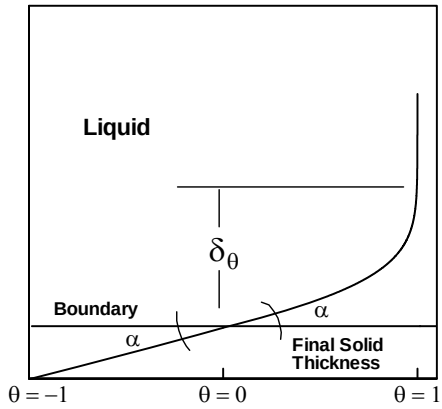

Fig. 2. b Final solid thickness, High *Pr* number.

According to this figure, there is a difference in ultimate solid thickness between two-dimensional and three-dimensional cases, as expected; however, the trend of evolution is the same in both graphs. In addition, the exact solution of energy equation can be used for validation of the numerical solution of the same equation. Figure 8 shows the comparison between exact and numerical solutions of temperatures profiles. Indeed, the exact solution is a quasi steady solution of the energy equation. This means the numerical solution is the same as the exact solution if there is enough time for evolution while other conditions are maintained constant. In this figure, two profiles are matched completely, at first and last times. At the beginning, the time of evolutions is very small and differences between these two profiles are negligible (two profiles are matched completely). At the end, there is enough time to complete the evolution of temperature profile while variations of other parameters are not considerable as they are very close to reach their steady conditions. In the middle times, there is a noticeable difference between two profiles expectedly; however, the trend of the profiles evolution at both figures is the same.

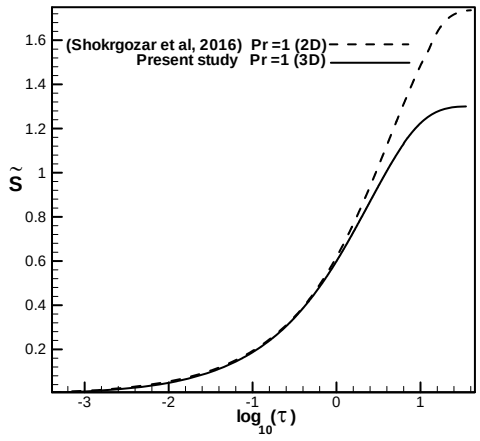

Fig. 3. Comparison of Two-dimensional (Shokrgozar *et al.*, 2016) and Three-dimensional (Present Study) results for $(Pr = 1, St = 1, K_r = 1, \alpha_r = 1, \theta_I = 1)$.

Figure 4 represents the temperature profiles of liquid and solid phases for different times due to advancement of solidifying front. The slope of each chart is $tg(\alpha)$ in the first node of liquid or solid phase. The figure reveals that solidification is stopped just as values of these two slopes become equal (note that $\alpha_r = 1$). Figure 5 presents the exact solution of thermal profile for different times and different solidification front velocity. Next, Figures 6 , and 7 provide the velocity profiles in r and z directions for different times and solid thicknesses. As it is shown, when the solidification velocity is very high, that is just for initial moments, the slope of velocity profile in boundary layer is very steep and the velocity approaches toward potential flow very fast and so the thickness of viscous boundary layer is very thin. By decreasing solidification velocity, Hiemenz flow is appeared more and more. Also, a comparison is made in Fig. 8 between exact and numerical solutions of heat transfer profiles at different times.

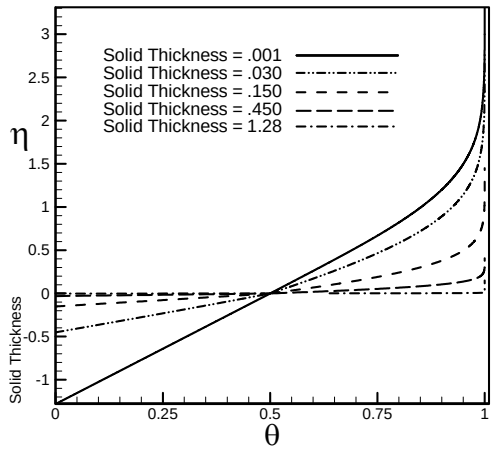

Fig. 4. Numerical solution, Thermal liquid and solid profiles for $(Pr = 1, St = 1, K_r = 1, \alpha_r = 1, \theta_I = 1)$.

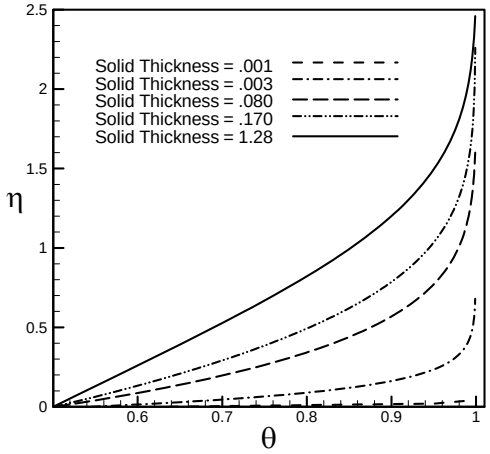

Fig. 5. Exact solution, Thermal profile for $(\Pr = 1, St = 1, K_r = 1, \alpha_r = 1, \theta_I = 1)$.

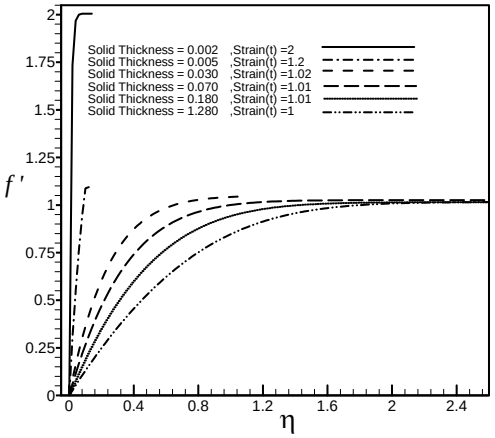

Fig. 6. Velocity profile in x **direction for** $(Pr = 1, St = 1, K_r = 1, \alpha_r = 1, \theta_I = 1)$.

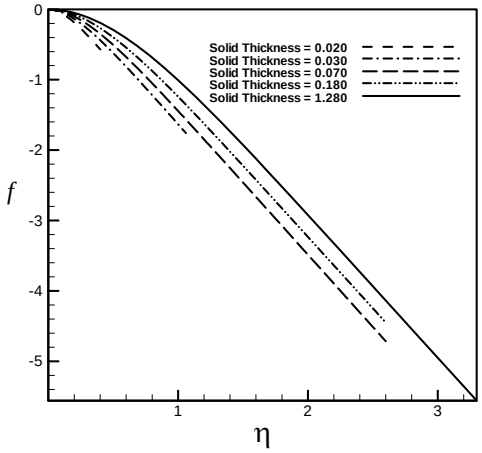

Fig. 7. Velocity profile in z **direction for** $(Pr = 1, St = 1, K_r = 1, \alpha_r = 1, \theta_I = 1)$.

6. PARAMETRIC STUDY

The parametric studies are applied for different values of $Pr, St, \theta_I, K_r, \alpha_r$ while study is concentrated on the advancement of solidifying front versus time that is the most important

phenomenon in solidification. In Fig. 9, a comparison is made between the solidification process of this study and Ref. (Shokrgozar *et al.*, 2013) for $Pr=1$, $Pr=10$ and $Pr=0.1$, respectively. The trend is the same in the two graphs so the solid upper limit decreases as Pr number increases relatively to basic $Pr=1$ graph. Mathematical analysis can confirm the validity of the numerical solution. Solidification will stop when the steady conduction heat transfer establishes in intersection. One-dimensional steady conduction heat transfer at intersection reads:

$$\Delta\tau = \frac{Pr.\Delta\tilde{z}^2}{St}\frac{1}{\theta_{liquid}+\theta_{solid}/\alpha_r} \tag{24}$$

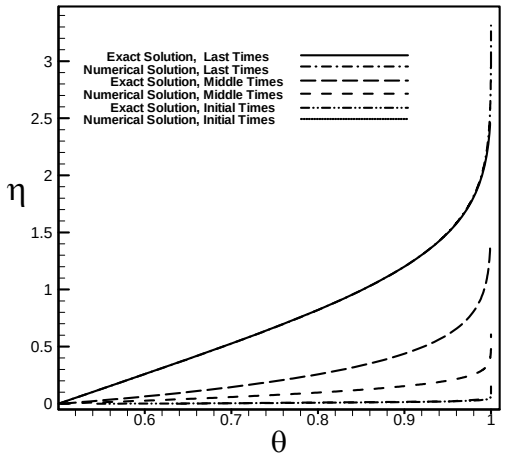

Fig. 8. Comparison between temperatures profile of exact solution and numerical solution $(Pr=1, St=1, K_r=1, \alpha_r=1, \theta_I=1)$.

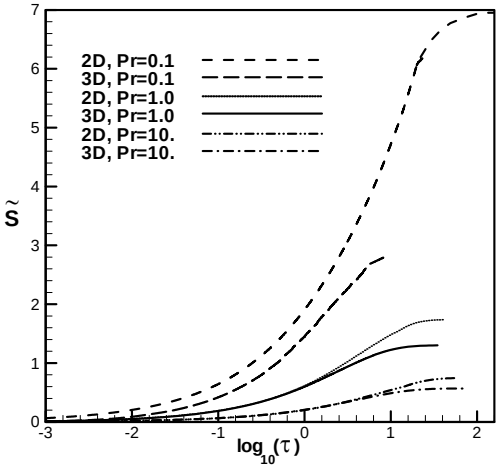

Fig. 9. Comparison between Two-dimensional and Three-dimensional. Effect of Pr number upon Solidification front for $(St=1, K_r=1, \alpha_r=1, \theta_I=1)$.

that the just upper and lower nodes temperature in fluid and solid regions are introduced by θ_{liquid} and θ_{solid}, respectively. In this equation, dimensionless time ($\Delta\tau$) tends to infinity as $(\theta_{liquid}+\theta_{solid}/\alpha_r)\to 0$ and solidification is stopped consequently while $\alpha_r=1$ is assumed for simplification. It can be referred to (Shokrgozar *et al.*, 2013) for more details. Figures 2A, and 2B determine the ultimate solid thickness that is equal to $tg(\alpha)$ (where $tg(\alpha)$ is slope of temperature profile at first node). It is evident that when the thickness of the temperature boundary layer increases, the solid upper limit increases and this increasing is due to Pr number decrease and vice versa. Moreover, it was capture that by taking into account solely the effect of St number does not change the solid upper limit as St number does not appear in (24) but St number variations changes the solidification time. However, a complete match of the heat transfer profiles obtained by two methods of exact solution and numerical solution at the beginning and ending times can be considered as the best reason for validation of the numerical results.

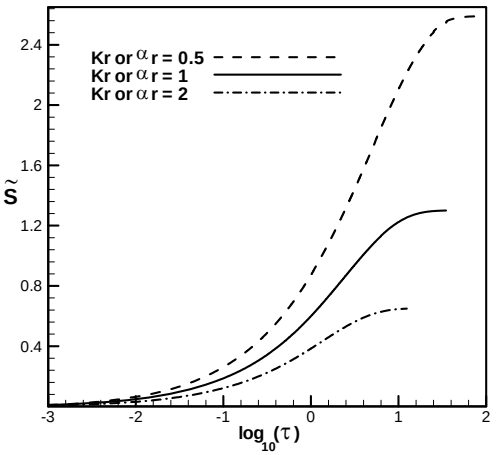

Fig. 10. Effect of k_r or α_r variations upon Solidification front for $(Pr=1, St=1, \theta_I=1)$.

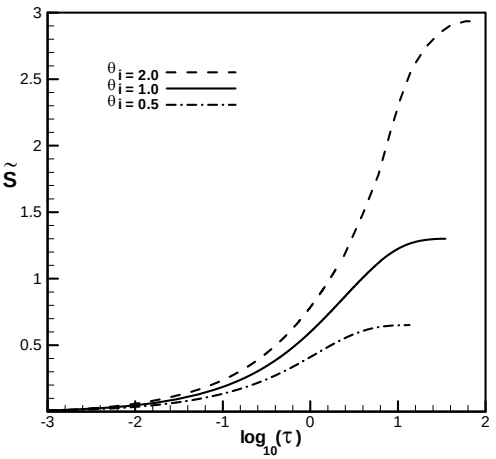

Fig. 11. Effect of θ_I variations upon Solidification front for $(Pr=1, St=1, K_r=1, \alpha_r=1)$.

Equation (24) shows that decreasing of k_r or α_r by half, increases solid upper limit two times exactly of that $tg(\alpha)$ increases two times (figure 2). Also, Figure 10 shows the effect of k_r and α_r variations upon solidification front thickness. In this case, decreasing of k_r and α_r by half, increases thickness of solid two times exactly. Figure 11 represents results for $\theta_I = 0.5$ and $\theta_I = 2$ ($Pr = 1, St = 1, k_r = 1, \alpha_r = 1$). The variations of θ_I have interesting results. When θ_I tends to zero, ultimate frozen thickness tends to infinity and this case requires another study separately. Figure 12 represents effect of Pr number variations in front solidification more clearly. As previously mentioned, this figure shows increasing Pr number decreases solid upper limit and vice versa. Figure 13 represents St number has no effect on the ultimate thickness in front solidification as former discussion. However the St number has only effect upon the solidifying time.

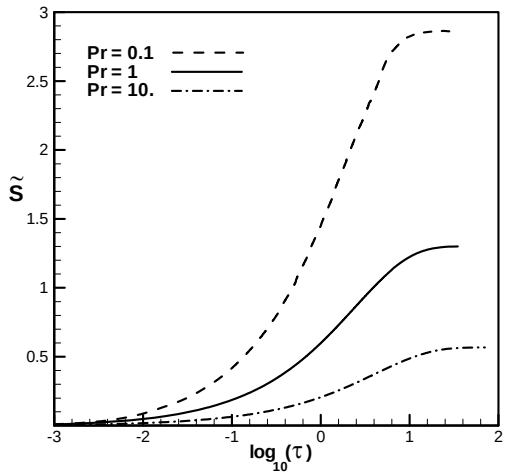

Fig. 12. Effect of Pr number upon Solidification front for $(St = 1, K_r = 1, \alpha_r = 1, \theta_I = 1)$.

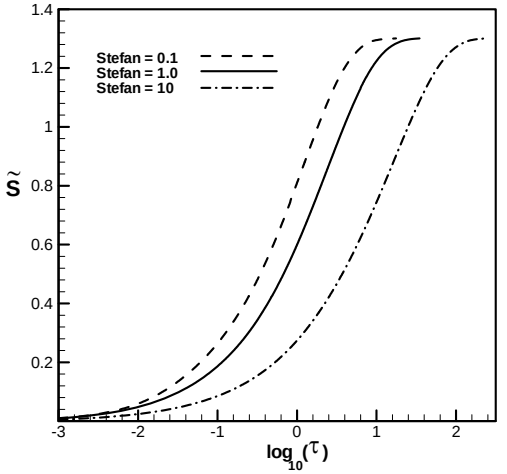

Fig. 13. Effect of St number upon Solidification front for $(Pr = 1, St = 1, K_r = 1, \alpha_r = 1)$.

7. CONCLUSIONS

An investigation of solidification modeling of a viscous stagnation three-dimensional flow on a flat plate is performed in this study. Solution approaches comprise: 1- Exact solution for momentum equations, 2-Numerical solution for the energy equation in liquid phase and solid-liquid interface and then 3-Exact solution for the energy equation in liquid phase as a quasi steady solution for validation of numerical solution of the energy equation. These equations are solved at any time step simultaneously.

The results show steady temperature boundary layer or, by more exact words, start of steady temperature profile slope determines the ultimate solidification thickness. Of course the steady temperature profile slope cans not be determined initially. However, the exact solution of energy equation is used to determine the steady temperature profile at the first. So we will know the ultimate thickness of solid before numerically solving the energy equation. The ratio of liquid to solid temperature diffusivity and, more importantly, Pr number has effect upon this temperature boundary layer thickness. This study represents increase of Pr number brings about the decrease of the ultimate solidification thickness and increasing k_r and/or α_r by half increases this thickness two times and vice versa. Also, decrease of θ_I causes the solidification thickness to increase. On the other hand, St number variations have no influence on the ultimate solidification thickness; however, increase in the value of this dimensionless number resulted in decrease of the time of approach to this thickness). Very small effect of convection terms at near of interface leads to flatting solidification front but these terms are very important as approaching to the edge of boundary layer. In fact, existence of these terms causes the solidification in a stagnation flow to be stopped. The results show that the final solid thickness in a three-dimensional stagnation flow is about 0.75 times of that of a two-dimensional case. Indeed, the exact solution of energy equation is a quasi steady solution and, therefore, its results can be used for validation of the numerical solution. This final result is very important because it is meaning of exact solution for the energy equation, in this case. This is an ingenious way of comparison in the field of stagnation flow.

REFERENCES

Brattkus, k. and S. H. Davis (1988). Flow induced morphological instabilities: stagnation-point flows. *Journal of Crystal Growth* 89, 423-427.

Curtic, M. O. and F. J. Spera (1992). Hybrid model for solidification and convection. *Numer. Heat Transfer* B 21, 217-229.

Goodrich, L. E. (1978). Efficient numerical technique for one dimensional thermal problems with phase change. *Int. Journal of Heat Mass Transfer* 21, 615-621.

Hadji, L. and M. Schell (1990). Interfacial pattern formation in the presence of solidification and thermal convection. *Phy. Rev*. A 41, 863-873.

Hanumanth, G. S. (1990). Solidification in the presence of natural convection. *Int. Comm. Heat Mass Transfer* 17, 283-292.

Joo-Sik, Y. (2000). Effect of viscous plane stagnation flow on the freezing of fluid. *Int. Journal of Heat and Fluid Flow* l(21), 735-739.

Lacroix, M. (1989). Computation of heat transfer during melting of a pure substance from an isothermal wall. *Numer. Heat Transfer* B 15, 191-210.

Lambert, R. H. and R. H. Rangel (2003). Solidification of a supercooled liquid in stagnation-point flow. *Int. Journal of Heat Mass Transfer* 46, 4013-4021.

Marchi, C. S., H. Liu, E. J. Laverniaand and R. H. Rangel (1993). Numerical analysis of the deformation and solidification of a sigle droplet impinging on to a flat substrate. *Journal Mater*. 28, 3313-3321.

Rangel, R. H. and X. Bian (1994). The inviscid stagnation-flow solidification problem. *Int. Journal of Heat Mass Transfer* 39(8), 1591-1602.

Shokrgozar, A. and A. B. Rahimi (2012). Investigation of Two-dimensional unsteady stagnation point-flow and heat transfer impinging on an accelerated flat plate. *Journal of Heat Transfe*r 134, 064501-5.

Shokrgozar, A. and A. B. Rahimi (2013). Solidification of Two-Dimensional viscous, incompressible Stagnation flow. *Int. Journal of Heat Transfer* 135, 072301-8.

Shokrgozar, A., A. B. Rahimi and H. Mozayyeni (2016). Investigation of three-dimensional axisymmetric unsteady stagnation point-flow and heat transfer impinging on an accelerated flat plate. *Journal of Applied Fluid Mechanics* 9, 451-461.

Sparrow, J., W. Ramsey and S. Harris (1983). The transition from natural convection controlled freezing to conduction controlled freezing. *Journal of Heat Transfer* 103, 7-13.

Stefan, J (1891). About the theory of ice formation, in particular on the ice formation in polar seas. A. Phys. Chem. 42, 269-286.

Trapaga, G. and E. F. Matthys and J. J. Valecia and J. Szekely (1992). Fluid flow, heat transfer and solidification of molten metal droplets impinging on substrates: comparison of numerical and experimental results. *Metall. Trans.* B 23B, 701-718.

Watanabe, T., I. Kuribayashi and T. Honda and A. Kanzawa (1992). Deformation and solidification of a droplet on a cold substrate. *Cham. Engng.* 47, 3059-3065.